Electronic Supplementary Information (ESI) for

Elucidating Synergistic Mechanisms of Anion–Cation Electrolyte Additive for Ultra–Stable Zinc Metal Anodes

Chenbo Yuan,[a] Jin Xiao,[a] Cong Liu,[a] and Xiaowen Zhan[a]*

[a]School of Materials Science and Engineering, Key Laboratory of Structure and Functional Regulation of Hybrid Materials of Ministry of Education, Anhui University, 230601 Hefei, Anhui, PR China

* Corresponding author
Email address: xiaowen.zhan@ahu.edu.cn (X.Z.)

Experimental Section

Materials

Commercial high–purity Zn foils (>99.999%, thickness: 0.1 mm) and Ti meshes (100 mesh, thickness: 0.3 mm) were obtained from Hengze Metals and Anping Kaian Metal Mesh Co., Ltd., respectively. Carbon cloth (WOS1011) was obtained from Suzhou Sinero Technology Co., Ltd. High–purity $ZnSO_4·7H_2O$ (99.995%, metal basis), NaF (99.99%, metal basis), NaCl (99.99%, metal basis), NaBr (99.99%, metal basis), NaI (99.99%, metal basis), aniline (99.5%, AR grade), ammonium persulfate (99.99% metal basis), and V_2O_5 (99.99%, metal basis) were purchased from Aladdin, while Na_2SO_4 (≥99.0%, AR grade) and HCl (AR grade, 12 M) were purchased from Sinopharm Chemical Reagent Co., Ltd.

Preparation of Electrolytes

The 2M $ZnSO_4$ solution was prepared by dissolving stoichiometric $ZnSO_4·7H_2O$ in 10 mL of deionized (DI) water. The modified electrolytes were obtained by mixing NaI with various concentrations (0.05 M, 0.1 M, 0.2 M, 0.5 M, 1 M and 2 M) into 2 M $ZnSO_4$ solution. Besides, to investigate the influence of halogen anions and alkali cation, the hybrid electrolytes were obtained by mixing 0.2 M NaF, 0.2 M NaCl, 0.2 M NaBr and 0.1 M Na_2SO_4 into 2 M $ZnSO_4$ solution. These electrolytes were named baseline electrolyte (BE), 0.05–NaI, 0.1–NaI, 0.2–NaI, 0.5–NaI, 1–NaI, 2–NaI, 0.2–NaF, 0.2–NaCl, 0.2–NaBr and 0.1–Na_2SO_4, where, for example, the BE represented 2 M $ZnSO_4$ and the 0.05–NaI represented hybrid electrolytes with BE and 0.05 M NaI.

Preparation of $NaV_3O_8·1.5\ H_2O$ Cathodes

$NaV_3O_8·1.5\ H_2O$ (NVO) cathode was synthesized according to previously reported method [1]. 1.5 g of V_2O_5 was dissolved into 50 mL of 2 M NaCl aqueous solution under magnetic stirring for 72 h at ambient temperature. The forming red gel was washed with DI and ethanol three times, and the final product was then dried at 80 °C overnight in a vacuum oven.

Fabrication of PANI@CC Cathodes

PANI@CC was synthesized through an *in–situ* polymerization method. Initially, 15 ml of 1 M HCl and 0.365 ml of aniline monomer were mixed under ice bath conditions, and then several pieces of carbon cloth (CC) with a diameter of 12 mm were immersed into the solution. After stirring for one hour, 5 mL of 1 M HCl containing 0.228 g of ammonium persulfate as a polymerization initiator was added. After one hour of continuous reaction, the solution turned

dark green indicating the completion of polymerization. Finally, the PANI@CC was obtained by washing with deionized water and alcohol.

Physicochemical Characterizations

The crystalline structure of the materials was investigated by X–ray diffraction (XRD) using an X–ray diffractometer (SmartLab 9 KW) in the 2θ range of 5–80° at a scan rate of 10° min^{-1}. The morphologies of Zn foils and NVO samples were detected employing a field emission scanning electron microscope (SEM, Hitachi, S–4800) and a Zeiss Crossbeam 550 SEM equipped with EDX detectors. Raman spectra were collected using a Via–Reflex Raman spectrometer with a 532 nm excitation laser. A Fourier transform infrared (FTIR) spectrometer (Thermo Fisher Nicolet iS50, American) was carried out to measure the spectra. The different electrolytes were investigated by ^{2}H nuclear magnetic resonance (^{2}H NMR) on a JNM–ECZ400S. The surface morphologies of Zn anodes with BE and 0.2–NaI electrolytes during the Zn plating process at 1 mA cm^{-2}/1 mAh cm^{-2} was monitored utilizing a Dino–Lite AM4113ZT microscope. The home–made optical cells were constructed with two Zn electrodes (length: 15 mm, width: 10 mm, thickness: 0.1 mm). A DSA30 Drop Shape Analyzer was applied to analyze the wettability of the BE and 0.2–NaI electrolytes on Zn foils. The ion conductivity test is performed using a PH/conductivity tester (LC–MP–31) from Lichen with a test temperature of 25 °C.

Electrochemical/Electroanalytical Measurements

The electrochemical properties were assessed using 2032–type coin cells collocated with a glass fiber separator (Whatman, GF/D), Zn foils (diameter: 12 mm) polished by P1200 sandpaper (in order to remove the passivation layer) and selected electrolytes. The NVO electrodes were prepared by mixing 70 wt% NVO, 20 wt% Super P, and 10 wt% PVDF binder. The average mass loading of NVO is ~3.7 mg cm^{-2}. Symmetrical cells and Zn||NVO/I full batteries were tested using a NEWARE–BTS battery tester, where the Zn||NVO and Zn||I batteries used cut–off voltage windows of respectively 0.3–1.25 V and 0.5–1.5 V. Before testing, all batteries were rested for 8 h to ensure sufficient electrolyte wetting. A CHI 760E electrochemical workstation was employed to evaluate linear polarization, cyclic voltammetry (CV), and chronoamperometry (CA). All electrochemical impedance spectroscopy (EIS) measurements in a frequency range of 100 kHz–1 Hz and a voltage amplitude of 10 mV were performed using a Gamry Interface 1010E potentiostat/galvanostat.

Molecular dynamics (MD) simulations

The coordination structures of solvents, cations and anions in different electrolytes were simulated by molecular dynamics (MD) simulation. The partial charge of $ZnSO_4$ was calculated using Gaussian 16 code and the 6–311g(d,p) basis functions were applied[2]. The OPLS–AA force field[3]and MKTOP[4] were used to parametrize all atoms, such as the bond parameters, angle parameters and the dihedral angles, and so on. In system 1, the monomer ratio of $ZnSO_4$: water=2: 55.56 and 100 $ZnSO_4$, 2778 water molecules were randomly inserted into a cube box with a side length of 6.0 nm. In system 2, $ZnSO_4$: NaI: water =2: 0.2: 55.56 and 100 $ZnSO_4$, 10NaI and 2778 water molecule molecules were randomly inserted into a cube box with a side length of 6.0 nm, too. The MD simulations were performed in the GROMACS 2021 software package[5–7]. The steepest descent method was applied to minimize the initial energy for each system with a force tolerance of 1 kJ/(mol^{-1} nm^{-1}) and a maximum step size of 0.002 ps before MD calculations[8]. In all the three directions, periodic boundary conditions were imposed. Leapfrog algorithm was used to integrate the Newtonian equation of motion. The MD simulation was processed in an NPT ensemble and the simulation time was 20 ns. In NPT simulations, the pressure was maintained at 1 bar by the Berendsen barostat in an isotropic manner[9] and the temperature was maintained by the V–rescale thermostat at 298.15 K. The Particle–Mesh–Ewald (PME) with a fourth–order interpolation was used to evaluate the electrostatic interactions and whereas a cutoff of 1.0 nm was employed to calculate the short–range van der Waals interactions[10].

Density functional theory (DFT) calculation

We utilized a first–principles approach[11, 12] to conduct density functional theory (DFT) computations employing the generalized gradient approximation (GGA) with the Perdew–Burke–Ernzerhof (PBE) formulation[13]. Our methodology involved the use of projected augmented wave (PAW) potentials[14] to characterize the ionic cores and consider valence electrons. This was complemented by a plane wave basis set featuring a kinetic energy cutoff set at 450 eV.

To account for partial occupancies of the Kohn–Sham orbitals, we applied the Gaussian smearing method with a width of 0.05 eV. We ensured self–consistency of the electronic energy by stipulating an energy change threshold of smaller than 10^{-5} eV. In the process of geometry optimization, convergence was defined by an energy change less than 0.02 eV per Ångström ($Å^{-1}$). The description of weak interactions involved the DFT+D3 method with an empirical correction within Grimme's scheme[15, 16].

The surface electrostatic potential between different particles was calculated by gaussian, where b3lyp/6–311g(d,p) was used for optimization and frequency calculation, b3lyp/6–311++g(d,p) was used for single point energy calculation, SMD was used for implicit solvent model to investigate solvent atmosphere, and b3lyp/aug–cc–pVDZ–PP was used for optimization and frequency calculation and single point energy calculation of I^- ions. The binding energy between different particles was also calculated by gaussian, where b3lyp/6–311g(d,p) was used for optimization calculation, b3lyp/6–311+g(d,p) was used for single point energy calculation, SMD was used for implicit solvent model to investigate solvent atmosphere, and b3lyp/aug–cc–pVDZ–PP was used for optimization and single point energy calculation of I^- ions.

Finite Element Analysis

Based on the finite element method, the current density and Zn^{2+} concentration were modeled by the commercial COMSOL Multiphysics 5.6, which used a comprehensive simulation method coupled with the "Deformable geometry" and "Tertiary current distribution" modules. This approach revealed the electrochemical reaction process of Zn^{2+} at the deposited interface as well as the surface deformation of the Zn anode. Consequently, neglecting the mass conservation of H^+ in the simulation and assuming complete ionization of $ZnSO_4$ into ions is permissible. The starting potential between the two electrodes was chosen at 0.1 V, and the electrode distance and length were both set to 3 µm. The bump generated by Zn^{2+} deposition on the surface of the Zn anode in BE is represented by five dome triangles (base height: ~300 nm and width: ~200 nm). Simultaneously, a chain of small protuberances reflects the stage of Zn^{2+} deposition on the Zn anode with the help of 0.2–NaI. This simulation could determine the transient change process of the ion concentration field by calculating the Nernst–Einstein equation when the working current was applied. The galvanostatic current density was chosen at 10 mA cm^{-2}. The Zn^{2+} diffusion coefficient in the electrolyte was fixed to $3.3 \times 10^{-10} m^2 s^{-1}$. The simulation model's computational domain was developed using the findings of in–situ optical microscopes, SEM, AFM images, as well as the model's viability.

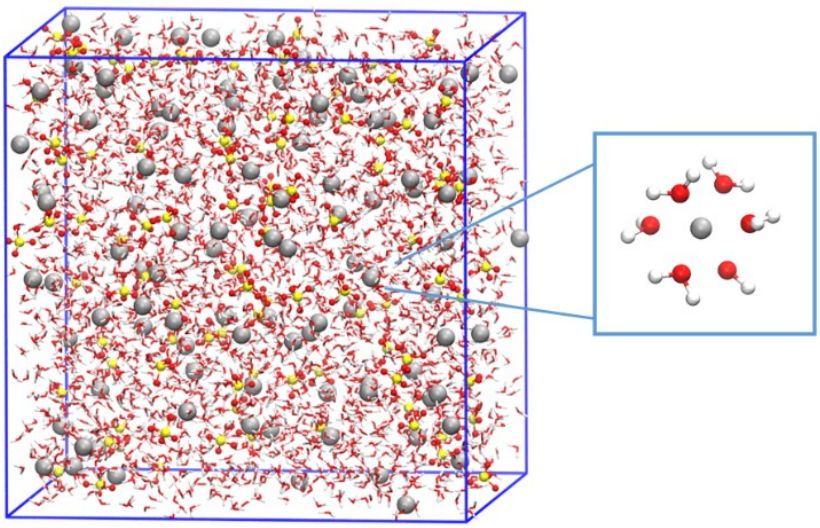

Figure S1. 3D snapshots of BE system obtained from MD simulations and partially enlarged snapshots of the solvation structure of Zn^{2+}.

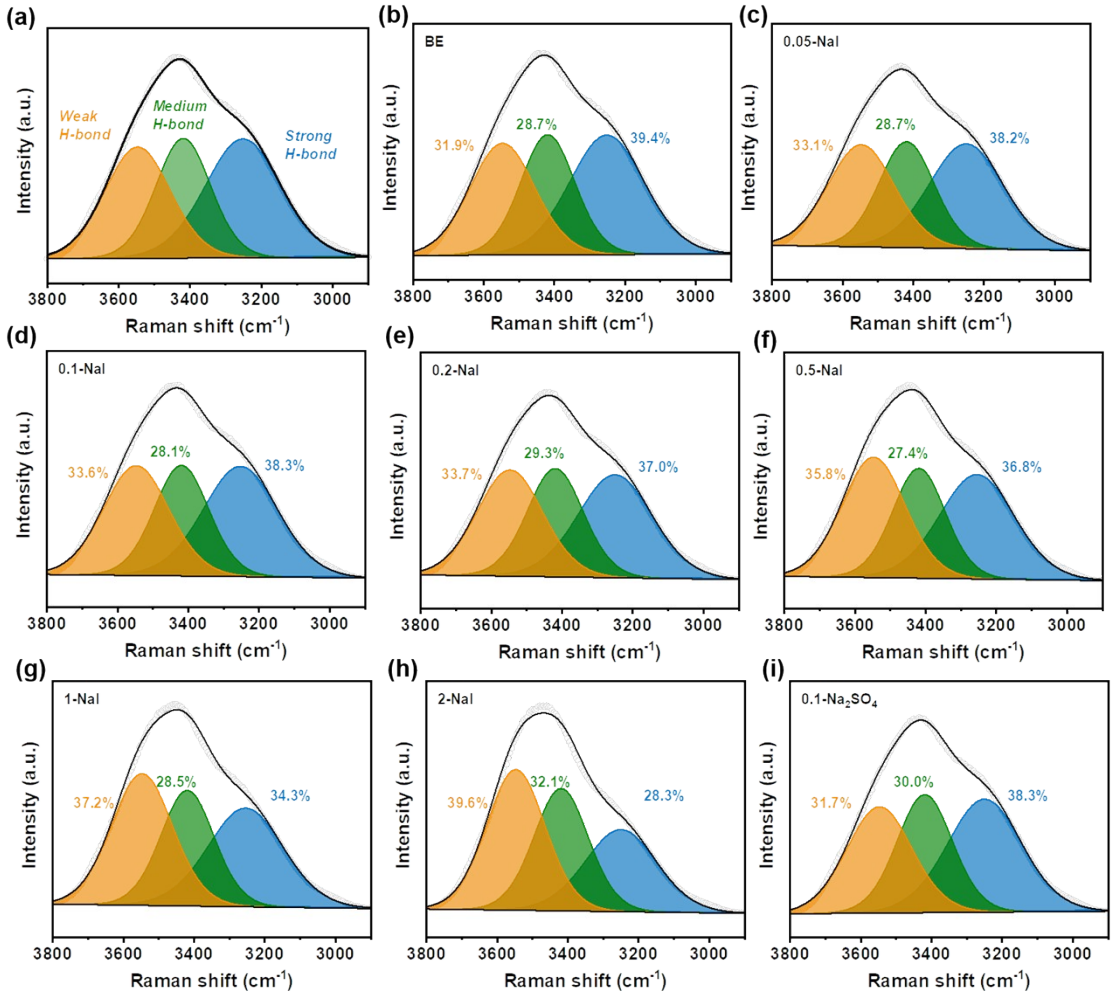

Figure S2. Raman spectra and corresponding fitted curves of selected electrolytes: (a) BE, (b) 0.05–NaI, (c) 0.1–NaI, (d) 0.2–NaI, (e) 0.5–NaI, (f) 1–NaI and (g) 2–NaI.

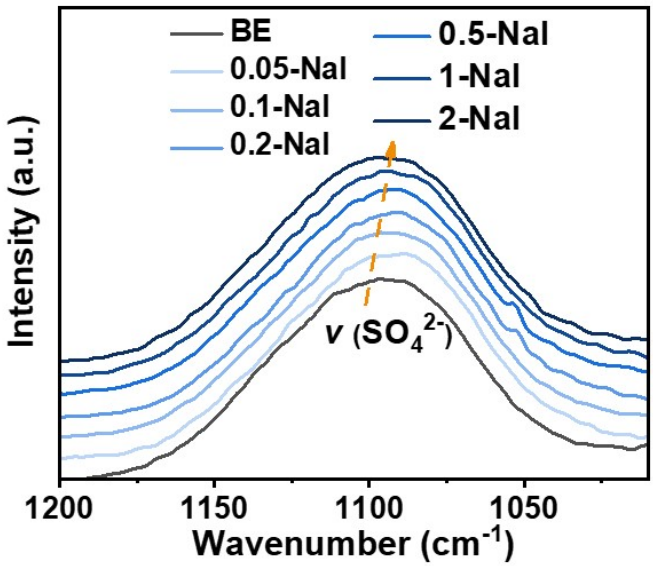

Figure S3. FT–IR spectra of selected electrolytes correspond to SO_4^{2-} stretching vibration.

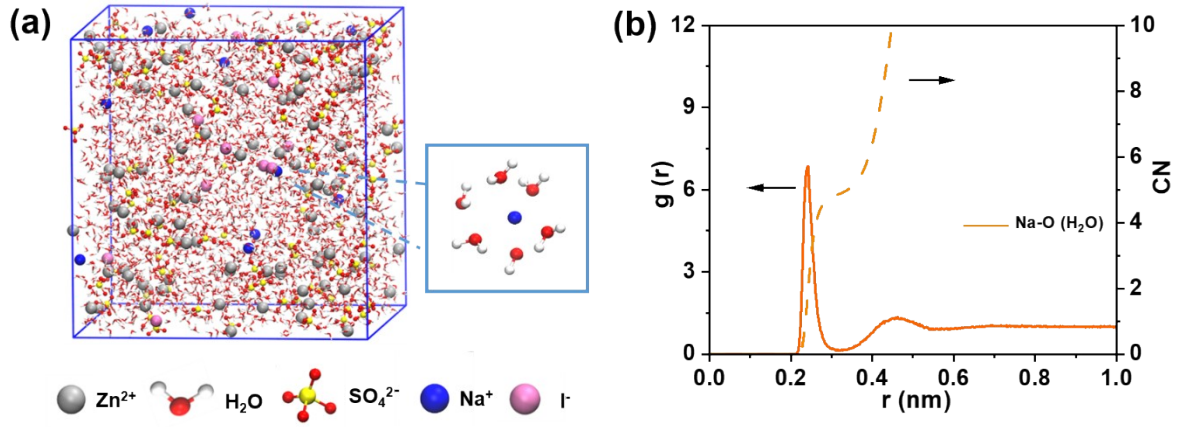

Figure S4. (a) 3D snapshots of 0.2–NaI system obtained from MD simulations and partially enlarged snapshot of the solvation structure of Na^+. (b) RDF and CN for Na–O (H_2O) collected from MD simulations in 0.2–NaI system.

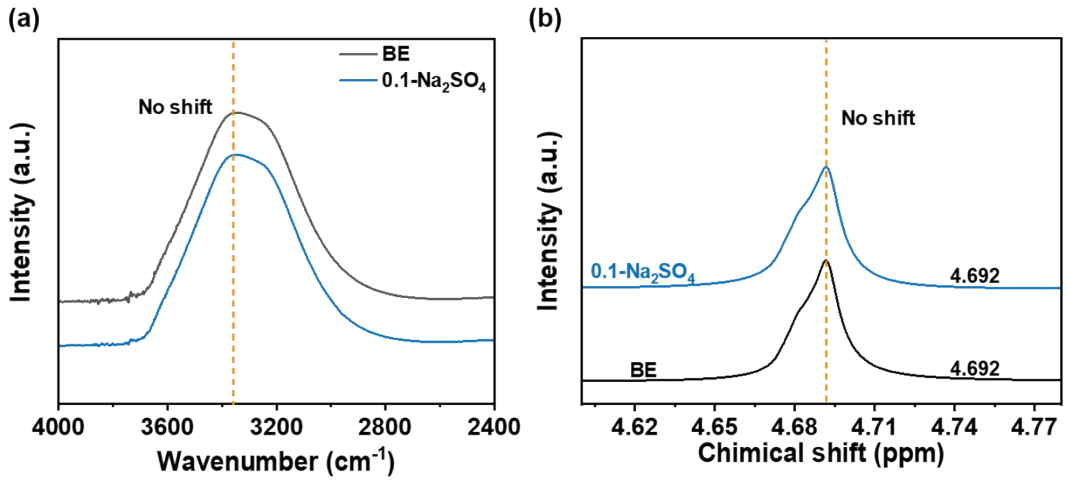

Figure S5. (a) FTIR and (b) ^2H NMR spectra for BE and 0.1–Na_2SO_4 electrolytes.

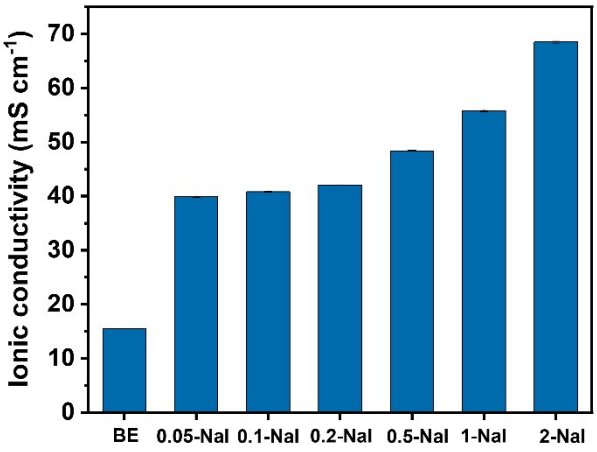

Figure S6. Ionic conductivities of BE and various concentrations NaI electrolytes at 25 °C.

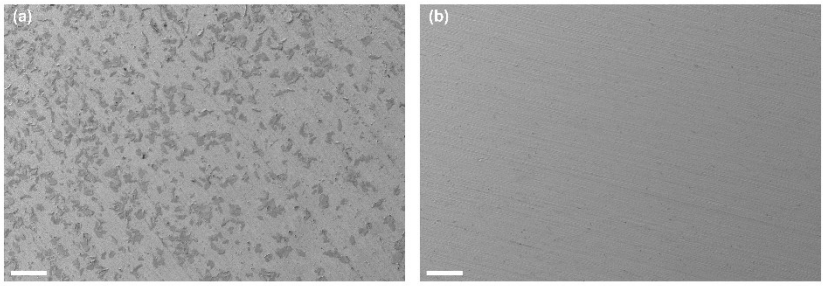

Figure S7. SEM images of Zn anodes after resting 14 days in (a) BE and (b) 0.2–NaI electrolytes. Scale bars: 200 μm.

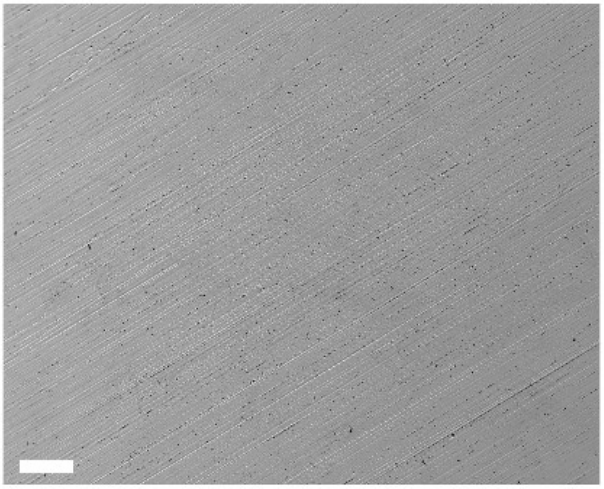

Figure S8. SEM image of the polished Zn foils. Scale bar: 200 μm.

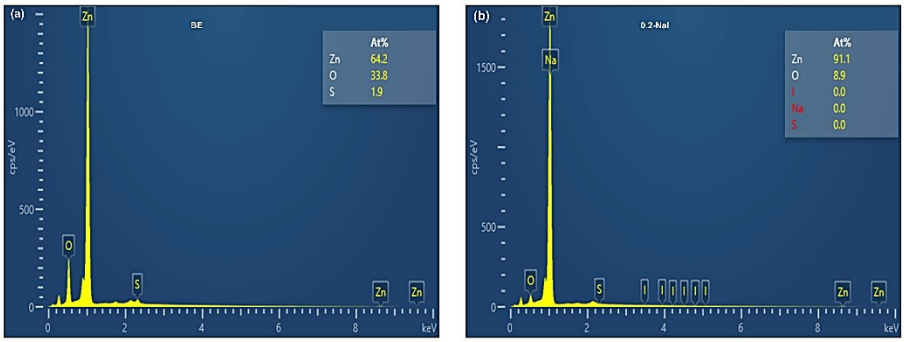

Figure S9. Map sum spectra of Zn anodes after resting 14 days in (a) BE and (b) 0.2–NaI electrolytes.

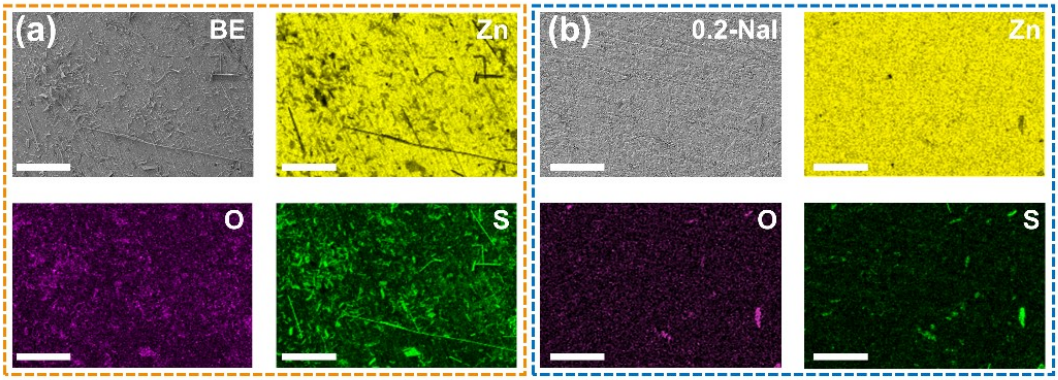

Figure S10. SEM and corresponding EDS mapping images of Zn anodes after 45 cycles in (a) BE and (b) 0.2–NaI electrolytes. Scale bars: 50 µm.

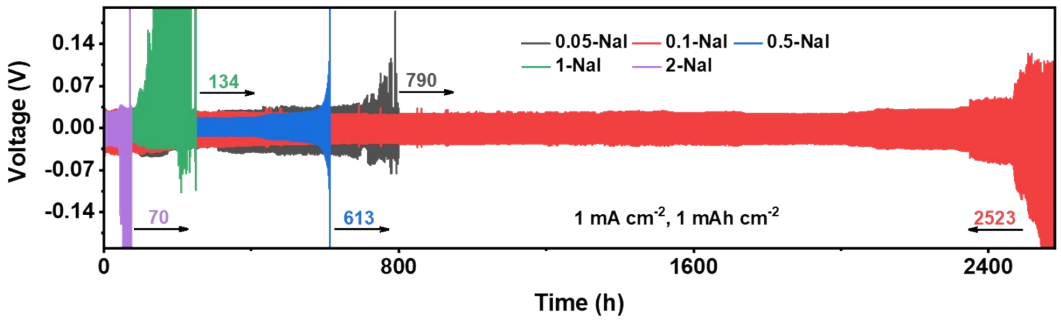

Figure S11. Galvanostatic cycling performance of symmetrical cells at 1 mA cm^{-2}/1 mAh cm^{-2} with different electrolytes.

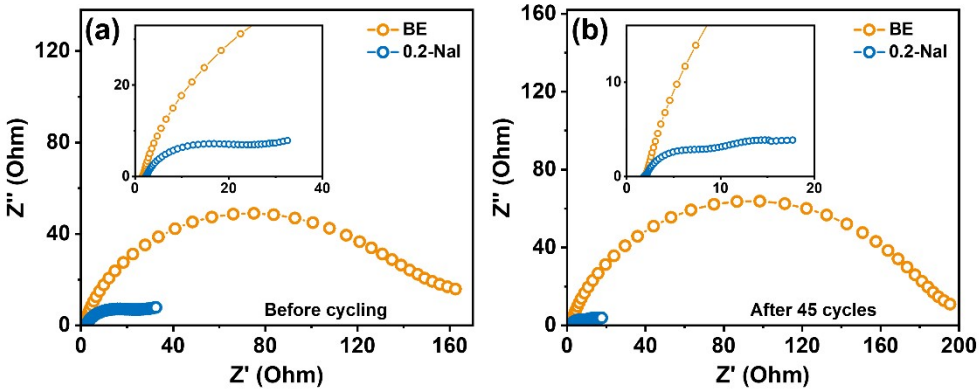

Figure S12. Nyquist plots of Zn symmetric cells using BE and 0.2–NaI electrolytes: (a) before cycling and (b) after 45 cycles at 1 mA cm^{-2} for 1 mAh cm^{-2}.

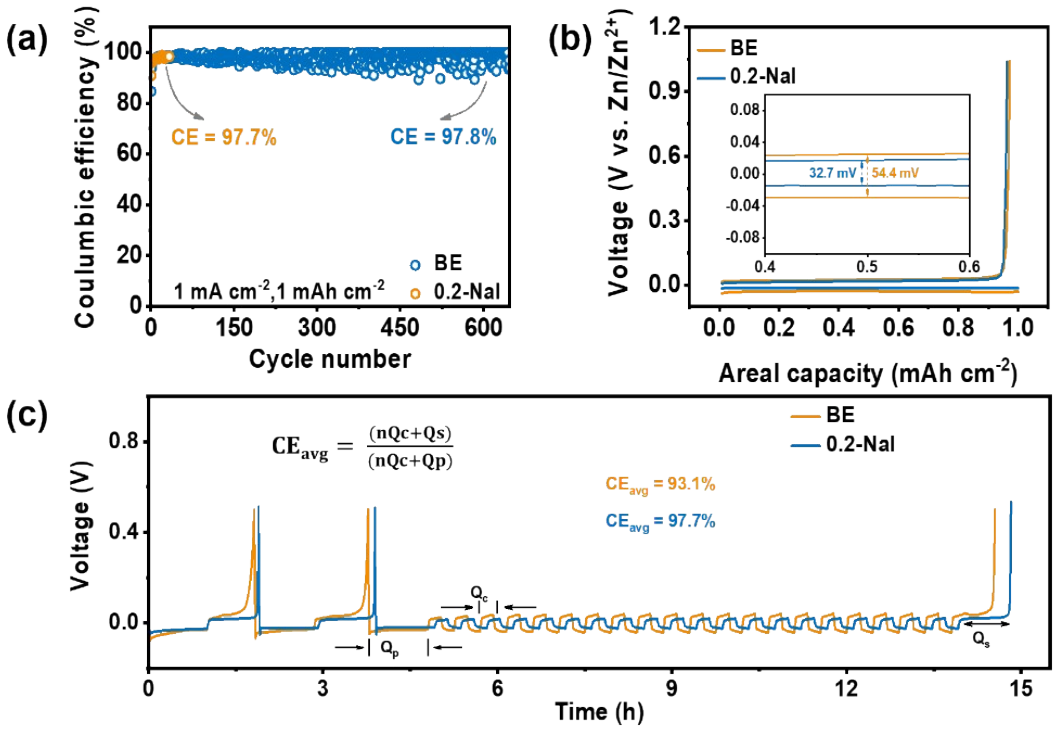

Figure S13. (a) CE of Zn||Ti cells in the BE and 0.2–NaI electrolytes at 1 mA cm^{-2}/1 mAh cm^{-2} and (b) corresponding expanded voltage profiles for the 3rd. (c) CE of Zn||Ti cells in BE and 0.2–NaI electrolytes at 1 mA cm^{-2}/1 mAh cm^{-2} based on a 'reservoir half–cell' method.

Figure S14. Digital photos of the BE, 0.2–NaF, 0.2–NaCl, 0.2–NaBr, 0.2–NaI and 0.1–Na_2SO_4 electrolytes (from left to right).

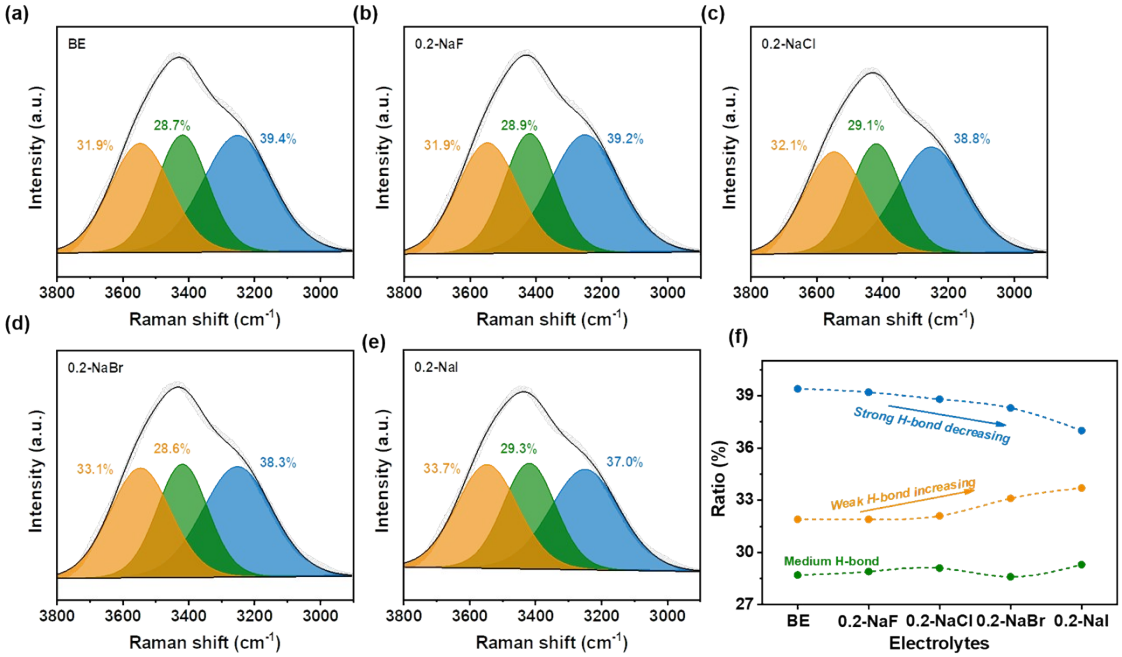

Figure S15. Raman spectra and corresponding fitted curves of selected electrolytes: (a) BE, (b) 0.2–NaF, (c) 0.2–NaCl, (d) 0.2–NaBr and (e) 0.2–NaI, (f) The ratios of *strong H–band*, *weak H–band*, and *medium H–band*

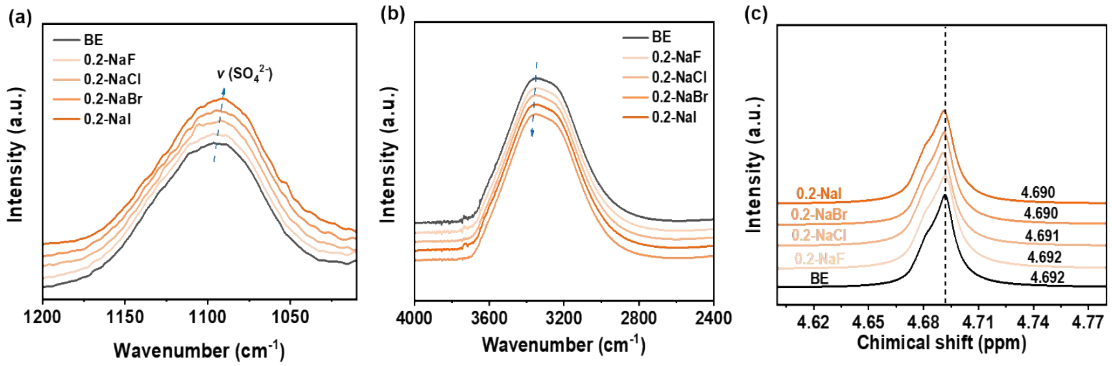

Figure S16. FTIR spectra based on stretching of (a) SO_4^{2-} and (b) O–H .(c) ^2H NMR spectra for selected electrolytes.

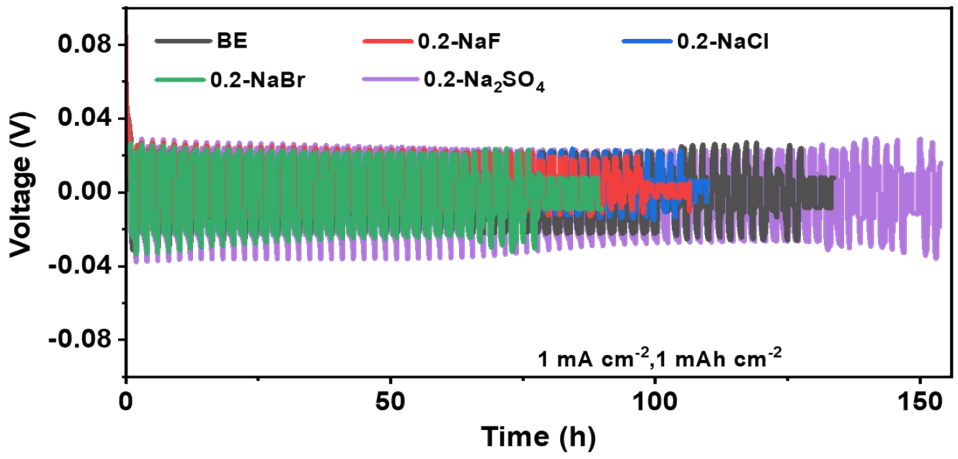

Figure S17. Galvanostatic cycling performance of symmetrical cells with different electrolytes at 1 mA cm^{-2}/1 mAh cm^{-2}.

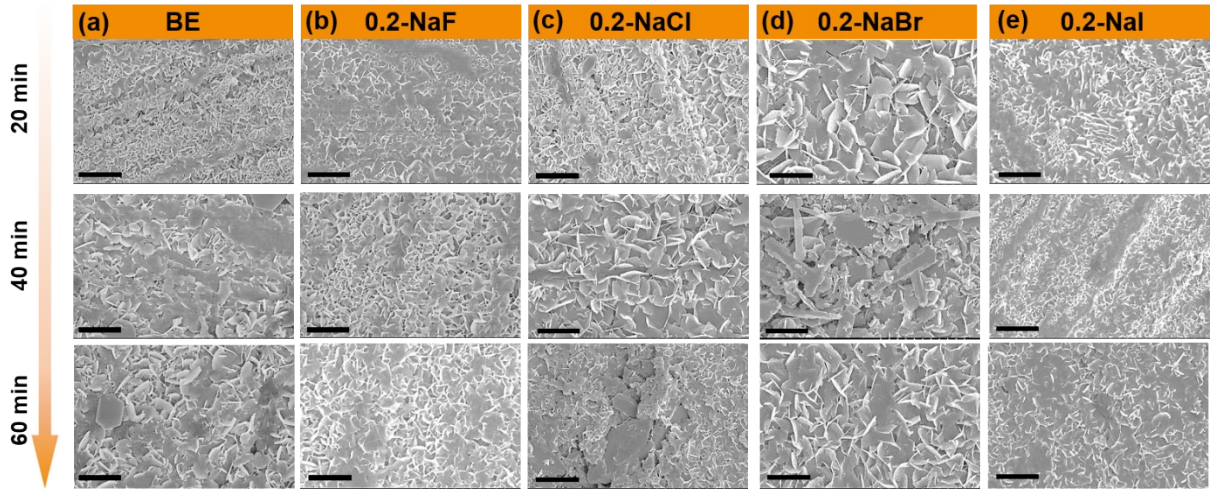

Figure S18. Morphology evolutions of Zn anodes at (a) BE, (b) 0.2–NaF, (c) 0.2–NaCl, (d)0.2–NaBr (e) 0.2–NaI and electrolytes during the initial Zn plating process with different duration.

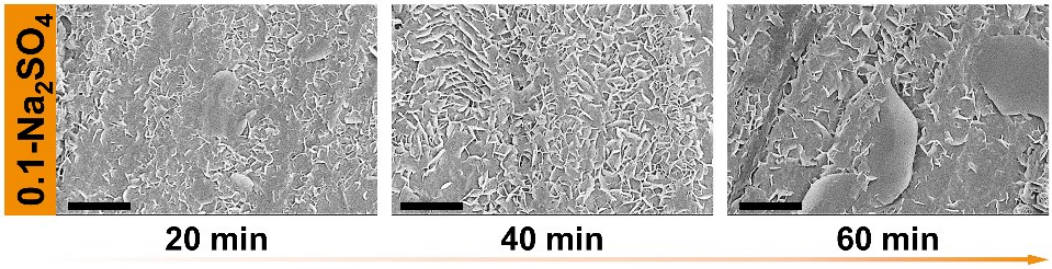

Figure S19. Morphology evolution of Zn anodes in 0.1–Na_2SO_4 electrolyte during the initial Zn plating process.

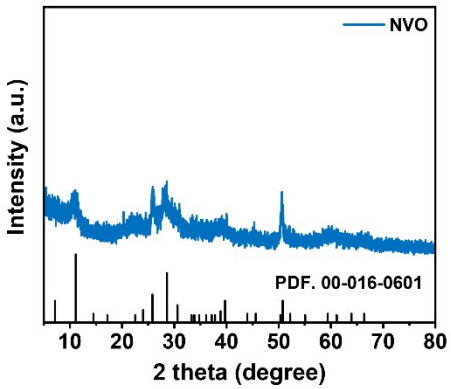

Figure S20. XRD pattern of the as–prepared NVO sample.

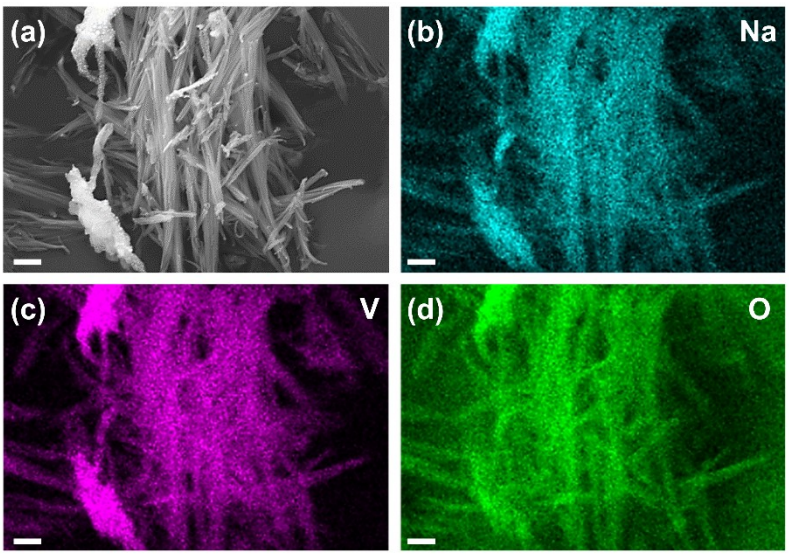

Figure S21. SEM and the corresponding EDS images of the as–prepared NVO sample. Scale bars: 500 nm.

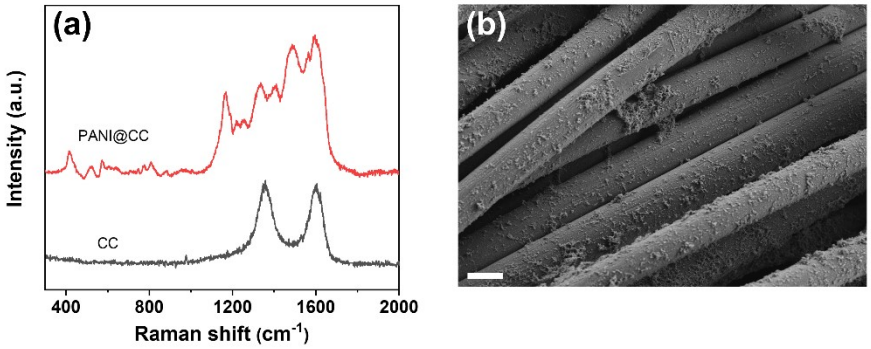

Figure S22. Raman spectra and SEM image of as–prepared PANI@CC cathodes.

Table S1. Primary EIS simulation parameters of Zn symmetrical cells in BE electrolytes at varying temperatures.

BE	R_s (Ω)	R_{SEI} (Ω)	R_{ct} (Ω)
30 ℃	2.053	174.3	516.1
40 ℃	1.708	46.83	192.2
50 ℃	1.902	65.84	140.3
60 ℃	2.034	59.44	96.55
70 ℃	1.99	48.14	58.15

Table S2. Primary EIS simulation parameters of Zn symmetrical cells in 0.2–NaI electrolytes at varying temperatures.

0.2–NaI	R_s (Ω)	R_{SEI} (Ω)	R_{ct} (Ω)
30 ℃	1.45	11.35	30.31
40 ℃	1.496	7.944	24.68
50 ℃	1.446	5.088	19.42
60 ℃	1.381	3.145	13.66
70 ℃	1.373	1.926	9.54

Table S3. Overpotentials of Zn symmetric cells in BE and 0.2–NaI electrolytes under different current densities and linear fits between overpotential and current density.

Current density	Overpotential η (mV)	
(mA cm^{-2})	BE	0.2–NaI
1	56.3	16.3
2	84.1	24.8
3	106.7	30.1
4	129.2	35.1
5	153.1	39.7
8	210.8	51.1
10	255.6	58.6
15	352.7	75.3
Linear fits	$\eta = 20.95\, i + 42.82$	$\eta = 4.06\, i + 17.01$

Note: The exchange current densities of symmetric cells with BE and 0.2–NaI were carefully calculated based on the formula $i = i_0 \frac{zF}{RT}\eta$, where i was the current density, i_0 was the exchange current density, η the overpotential, R and F the gas and Faradic constants, respectively, T the thermodynamic temperature and z the electron number involved in the electrode reaction (z = 2 in AZMBs).

Reference：

1 Q. Meng, R. Zhao, P. Cao, Q. Bai, J. Tang, G. Liu, X. Zhou and J. Yang, *Chem. Eng. J.*, 2022, **447**, 137471.

2 G. A. Petersson and M. A. Al-Laham, *J. Chem. Phy.* 1991, **94**, 6081–6090.

3 W. L. Jorgensen, D. S. Maxwell and J. Tirado–Rives, *J. Am. Chem. Soc.*, 1996, **118**, 11225–11236.

4 A. A. S. T. Ribeiro, B. A. C. Horta and R. B. d. Alencastro, *J. Braz. Chem. Soc.*, 2008, **19**, 1433.

5 D. Van Der Spoel, E. Lindahl, B. Hess, G. Groenhof, A. E. Mark and H. J. C. Berendsen, *J. Comput. Chem.*, 2005, **26**, 1701–1718.

6 M. J. Abraham, T. Murtola, R. Schulz, S. Páll, J. C. Smith, B. Hess and E. Lindahl, *SoftwareX*, 2015, **1–2**, 19–25.

7 H. J. C. Berendsen, D. van der Spoel and R. van Drunen, *Comput. Phys. Commun.*, 1995, **91**, 43–56.

8 W. F. Van Gunsteren and H. J. C. Berendsen, *Molecular Simulation*, 1988, **1**, 173–185.

9 B. Hess, H. Bekker, H. J. C. Berendsen and J. G. E. M. Fraaije, *J. Comput. Chem.*, 1997, **18**, 1463–1472.

10 M. Kawata and U. Nagashima, *Chem. Phys. Lett.*, 2001, **340**, 165–172.

11 G. Kresse and J. Furthmüller, *Comput. Mater. Sci.*, 1996, **6**, 15–50.

12 G. Kresse and J. Furthmüller, *Phys. Rev. B*, 1996, **54**, 11169–11186.

13 J. P. Perdew, K. Burke and M. Ernzerhof, *Phys. Rev. Lett.*, 1996, **77**, 3865–3868.

14 P. E. Blöchl, *Phys. Rev. B*, 1994, **50**, 17953–17979.

15 S. Grimme, J. Antony, S. Ehrlich and H. Krieg, *J. Chem. Phys.*, 2010, **132**.

16 S. Grimme, S. Ehrlich and L. Goerigk, *J. Comput. Chem.*, 2011, **32**, 1456–1465.